Profile Loss Prediction for Organic Rankine Cycle Turbines: An Experimental Case Study

Leander Hake *, Stephan Sundermeier, Stefan aus der Wiesche

Posted Date: 12 September 2023

doi: 10.20944/preprints202309.0738.v1

Keywords: Turbine; profile loss; organic Rankine cycle (ORC)

Article

Profile Loss Prediction for Organic Rankine Cycle Turbines: An Experimental Case Study

Leander Hake *, Stephan Sundermeier and Stefan aus der Wiesche

Muenster University of Applied Sciences, Department of Mechanical Engineering, Laboratory of Heat, Energy and Motor Technology, Campus Steinfurt, 48565 Steinfurt, Germany; Stephan.sundermeier@fh-muenster.de (S.S.); wiesche@fh-muenster.de (S.a.d.W.)

* Correspondence: leander.hake@fh-muenster.de (L.H.)

Abstract: Results of profile loss measurements, including trailing edge flow details, are presented for the flow of an organic vapor through a linear turbine cascade. The so-called VKI-I blade profile from the open literature was chosen for the cascade, and the working fluid was NOVEC 649. Pitot probes and hot wire anemometry were employed to measure the flow field up and downstream of the cascade. Details of the unsteady flow caused by the trailing edge of the blades and the turbulent spectrum were investigated using hot-wire anemometry. The new organic vapor flow results were compared with literature data obtained for air and with the prediction of conventional literature loss models. It was found that under certain thermodynamic conditions, specific traditional loss models can reasonably predict organic Rankine cycle (ORC) turbines' profile loss. Still, significant deviations between the loss models and the experimental data can also occur.

Keywords: turbine; profile loss; organic Rankine cycle (ORC)

1. Introduction

Since the pioneering work of Ainley and Mathieson [1], several different loss models and loss prediction systems have been developed for steam and gas turbines. Although sophisticated and complex computational fluid dynamics (CFD) methods are widely available, mean line models are still necessary for preliminary axial-flow turbines' design and optimization. Specific loss models can reasonably predict losses for steam and gas turbines under certain conditions. However, relatively little is known regarding their performance for organic Rankine cycle (ORC) turbines. The impact of the non-perfect gas behavior of the involved organic vapors needs to be addressed in conventional loss systems. The usual practice is to compute perfect gas equivalent input quantities for the loss model as done, for instance, by Harloff [2], and the conventional literature loss models or correlations are directly employed. In principle, the careless use of perfect gas quantities for calculating real gas phenomena is not free of fundamental difficulties. Besides the real gas behavior, there is also an additional problem in the experiments with the high molecular weight of the organic fluids and the resulting high-velocity regimes. The literature loss correlations have been established based on the typical Reynolds numbers, roughness levels, and turbulence length scales occurring in steam and gas turbines. Deviations might arise in ORC turbines due to the different ratios between turbulent length scales, roughness, and blade dimensions and their impact on flow separation and boundary layer development.

An inspection of the open literature shows that the conventional loss systems were applied to ORC turbines without any modification or experimental proof of their validity. Macchi and Perdichizzi [3] presented the results of an efficiency prediction study based on the Craig and Cox [4] correlation for axial-flow turbines operating with non-conventional fluids. Da Lio et al. [5] provided efficiency charts for the optimum design of axial flow turbines for organic Rankine cycles calculated using the Aungier [6] loss model. Sim et al. [7] employed the Kacker and Okapuu [8] loss model for their performance analysis of an ORC turbine. The selection of a specific loss model for ORC turbine

Preprints (www.preprints.org) | NOT PEER-REVIEWED | Posted: 12 September 2023 doi:10.20944/preprints202309.0738.v1

application seemed arbitrary in the current literature. The authors did not provide proper validation or a deeper fundamental reason for their choices or even ignored the possibility of erroneous loss models. In contrast to that attitude, Chyu and Young [9] found in their loss evaluation of a specific high-pressure rocket fuel pump turbine with a working fluid characterized by non-perfect gas behavior that "the correlations currently available in the literature may not be suitable for accurate loss prediction." Salah et al. [10] compared loss models in a theoretical study for air, sCO2, and ORC axial flow turbines, and they concluded that "the loss models can predict significantly different loss distributions." Furthermore, they pointed out that "to date there has been limited experimental data to provide sufficient validation that existing turbine models are suitable for these non-conventional working fluids."

Regarding the above issues, an experimental case study was conducted to assess the performance of frequently used loss prediction models for ORC turbines. This study focused on profile loss, including the trailing edge loss contribution, for a representative linear turbine cascade. Although secondary losses and tip clearance losses contribute to the total loss in actual turbine cascades, the profile loss still represents the basis loss for any model. It is hence a good starting point for more detailed future studies covering secondary flow phenomena and tip leakage flow. The experimental data of the present case study might also serve for validation purposes regarding computational fluid dynamics (CFD) methods. Since only a single cascade configuration was considered, the present study is incomplete because statements about any operation point and axial flow turbine cannot be drawn. It represents only a case study that illuminates literature loss models' potential and limitations when applied to ORC turbines.

2. Test model and fluid

The so-called VKI-I turbine cascade, frequently considered in the open literature, was selected as a test model for the present study. The nomenclature and primary cascade data are provided in Figure 1. The airfoil coordinates were well documented by Kiock et al. [11]. For this cascade, reliable literature data for high subsonic up to the transonic flow of air are available (Kiock et al. [11]).

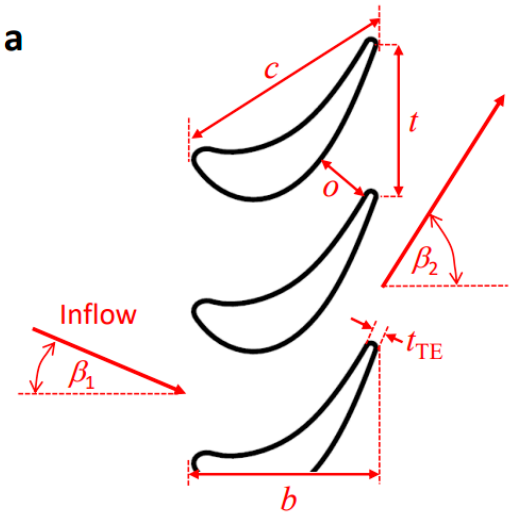

b

Spacing	t	22.0 mm
Chord	c	30.5 mm
Axial chord	b	25.0 mm
Throat	o	8.3 mm
Span	H	50.0 mm
TE thickness	t_{TE}	1.4 mm
Roughness	k_s/c	4×10^{-4}
Inflow	β_1	30°
Exit	$\cos^{-1}(o/t)$	67.8°

Figure 1. Considered turbine cascade: (a) nomenclature and (b) main actual parameters.

The planar stainless steel manufactured cascade, shown in Figure 1, is based on a classical cooled gas turbine airfoil design. For the present purpose, the relatively sizeable trailing edge thickness t_{TE} was advantageous because it enabled the inclusion of substantial trailing edge losses, which are relevant for ORC turbines, as Baumgärtner et al. [12] discussed. It was decided to use rough blades with an equivalent normalized sand grain roughness of $k_s/c = (4.0 \pm 0.5) \times 10^{-4}$ for the present case study (the standard finish of new blades would lead to levels about $k_s/c = 0.5 \times 10^{-4}$ up to 1.0×10^{-4}). The reasons for employing rough airfoils for the cascade were (i) it enabled a check of the roughness

Preprints (www.preprints.org) | NOT PEER-REVIEWED | Posted: 12 September 2023 doi:10.20944/preprints202309.0738.v1

correction of loss correlations and (ii) it represented realistic conditions for actual turbines in use (at least after aging). Further details about the manufacturing process and the roughness measurements for the present cascade can be found elsewhere (Hake et al. [13]). Hake et al. [13] recently published some experimental loss data focusing on roughness effects for the flow of an organic vapor through this cascade.

The non-toxic organic vapor NOVEC 649 (fluoroketone) by 3M was selected as a testing fluid. The molecular mass of Novec is 316 g/mol, and the critical point is at 18.8 bar and 442 K. The *h*-*s*-diagram of NOVEC 649, Figure 2a, demonstrates that this organic vapor is a dry fluid defined by an overhanging two-phase region. Its thermodynamic behavior represents a broad working fluid class for ORC power systems. The *Z*-*p*-diagram, Figure 2b, illustrates that NOVEC 649 is a non-perfect gas because its compressibility factor Z is not a unique function of the specific entropy s. If so, the (red) lines s = constant must be horizontals in Figure 2b, which is not the case. As discussed in detail by Traupel [14] or by aus der Wiesche and Reinker [15], a fluid with $Z = Z(s)$ is formally equivalent to a perfect gas in terms of turbine cascade aerodynamics. If this condition is violated, which is obviously for NOVEC 649 for pressures between 1 bar and 10 bar the case, its aerodynamics cannot be formally described by perfect gas dynamics. The operation points for the present case study were given by a constant stagnation temperature of T_o = 370 K and prescribed density levels of ρ = 30 kg/m³ and 16.5 kg/m³, respectively.

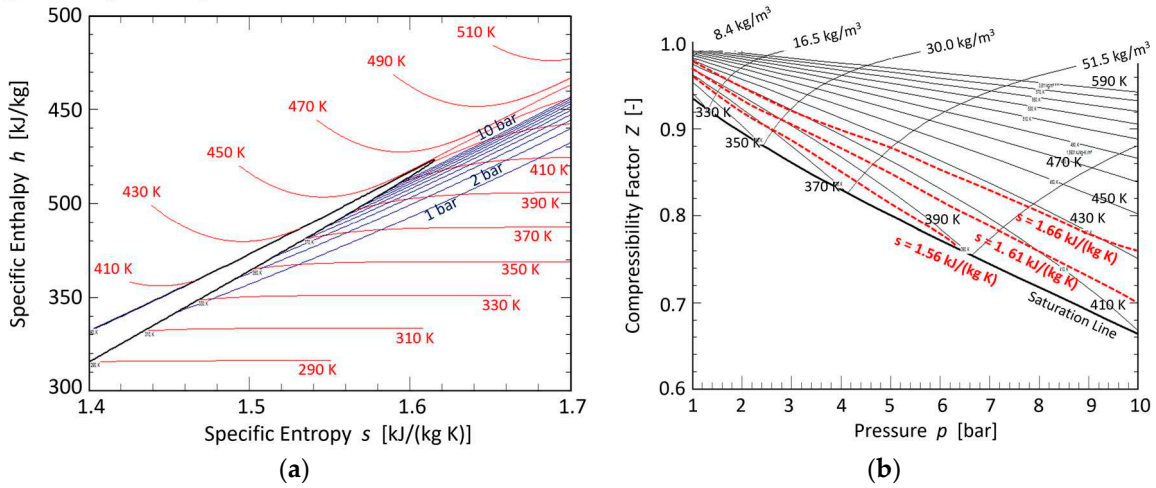

Figure 2. Thermodynamic behavior of NOVEC 649: (a) *h*-*s*-diagram and (b) *Z*-*p*-diagram (data obtained by REFPROP, NIST).

Table 1 compares the physical properties of air (at standard atmosphere conditions) and NOVEC 649. The thermodynamic properties for NOVEC 649 were evaluated using REFPROP at a pressure level of 2.5 bar and a temperature of about 97°C representing typical ORC operation and testing conditions. The significant difference between the isentropic exponents (i.e., the ratio of the specific heats) between air and NOVEC 649 is striking.

Table 1. Physical properties of air and Novec™ 649 (evaluated using REFPROP by NIST).

	Air	Novec™ 649
Pressure level p [MPa]	0.10	0.25
Temperature level T [K]	298	370
Density ρ [kg/m³]	1.17	28.46
Isentropic exponent γ[-]	1.40	1.05
Compressibility factor Z [-]	1.00	0.90
Fundamental derivative G [-]	1.20	0.94
Speed of sound a [m/s]	346.2	90.7

Preprints (www.preprints.org) | NOT PEER-REVIEWED | Posted: 12 September 2023 doi:10.20944/preprints202309.0738.v1

Dynamic viscosity η [Pa s]	1.85×10^{-5}	1.39×10^{-5}

The fundamental derivative of gas dynamics Γ is suitable for classifying gas dynamics [16]. A perfect gas exhibiting classical gas dynamics is characterized by $\Gamma = (\gamma + 1)/2$. This holds for dry air under atmospheric conditions. Classical but non-ideal gas dynamics correspond to $0 < \Gamma < 1$. This is achieved for NOVEC 649 under the thermodynamic conditions in Table 1. The existence of fluids exhibiting non-classical gas dynamical phenomena with $\Gamma < 0$ is still open [16].

3. Experimental setup

The present experimental investigation used the closed-loop organic vapor wind tunnel (CLOWT) at Muenster University of Applied Sciences, shown in Figure 3. Details about this test facility and its capabilities for cascade experiments can be found in a recent study (Hake et al. [13]) or in a review [16] of test facilities and measurement techniques for non-ideal compressible fluid dynamics.

A centrifugal compressor drove the working fluid through the closed-loop wind tunnel. The settling chamber was equipped with a chiller to maintain stable total temperature conditions during operation (during the start-up stage, the entire wind tunnel was electrically heated up to the desired temperature level). A multi-stage turbulence screen set and a two-stage contraction led to inflow turbulence levels of order 1 %. The turbulent macro length Λ (obtained by hot-wire anemometry, see following subsection) was of order 1 up to 2 mm in the test section. This corresponded to a normalized turbulent length scale Λ/c of order 3×10^{-2} up to 6×10^{-2}, much larger than the normalized roughness of $k_s/c = (4.0 \pm 0.5) \times 10^{-4}$. The linear turbine cascade was placed in the wind tunnel's test section. The details of the cascade test section of the present investigations are shown in Figure 4.

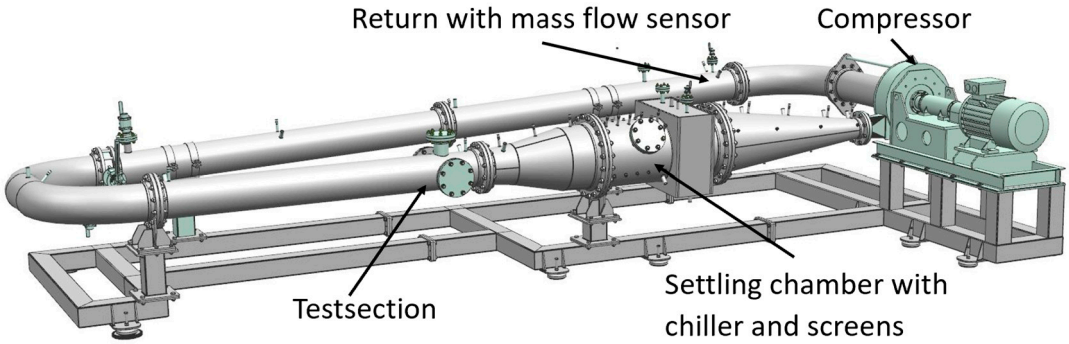

Figure 3. Closed-loop organic vapor wind tunnel (CLOWT) with its main components. The thermal insulation and the electrical heating system are not shown for simplicity.

Preprints (www.preprints.org) | NOT PEER-REVIEWED | Posted: 12 September 2023 doi:10.20944/preprints202309.0738.v1

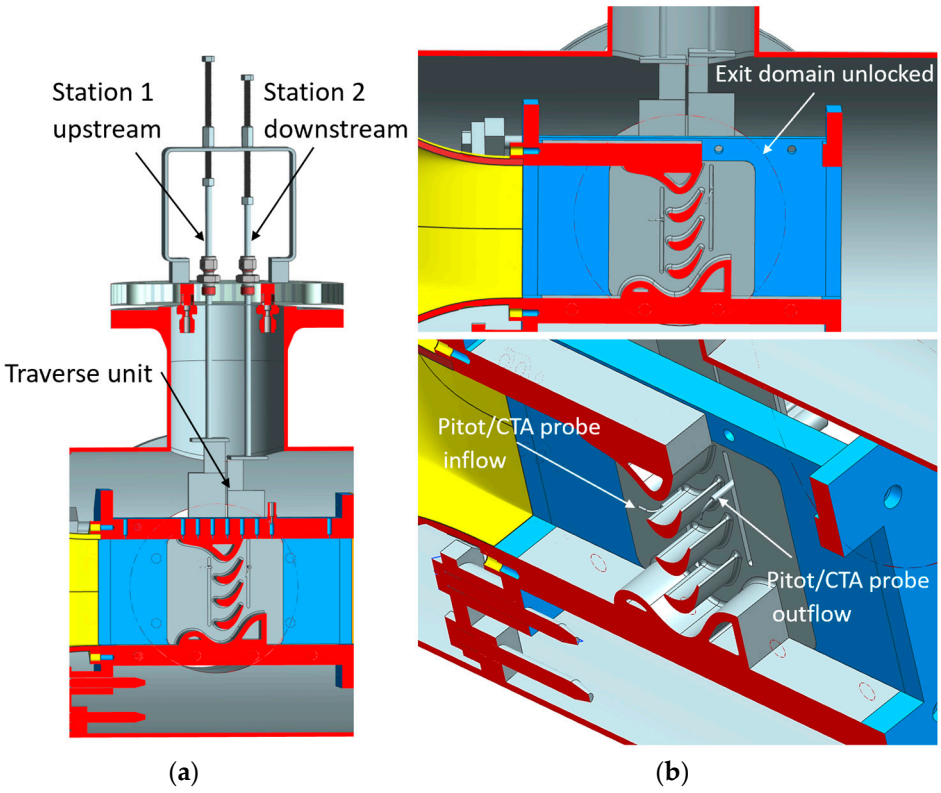

Figure 4. Cascade test section details: (a) installed traverse unit and (b) test section view.

The present work represents a direct continuation of the previous study [13] employing a modified cascade test section and new measurement techniques. The main differences to the previous study were: (i) the downstream domain of the cascade was significantly enlarged so that periodicity was ensured and the risk of a stagnation point flow at an end wall downstream of the cascade was prevented during the present measurements, (ii) profile pressure distributions were obtained for the airfoils, too, (iii) hot-wire anemometry was employed in addition to the pressure measurements, and (iv) the movement of the probes and potential vibration issues in the streams of the high-density organic vapors were observed using optical access to the cascade test section and employing a high-speed camera.

3.1. Instrumentation

The static pressure p_0 and the total temperature T_{o0} were measured at fixed positions in the wind tunnel's settling chamber (denoted by subscript *0*). During operation, the mass flow rate $\dot{m}$ was measured at the return of the closed-loop wind tunnel, see Figure 3. At the beginning of the high-speed test section (i.e., at the upstream station of the cascade denoted by subscript 1), the inflow static wall pressure p_1 was obtained through a static pressure tap placed centrally at the entrance of the cascade test section. Further static wall pressure taps were located at the end walls of the central blade passage of the cascade. Total pressures $p_{o1}(y)$ and $p_{o2}(y)$ were measured in the centerline of the cascade at upstream and downstream stations employing Pitot probes (tip diameter 1 mm, stem diameter 3 mm) along the traverse coordinate y. The upstream station 1 was placed one axial chord upstream of the blade leading edge. The axial distance of downstream station 2 to the trailing edge of the blades was $x/c = 0.07$.

In addition to the Pitot probes, hot-wire measurements were conducted using a single wire (length 4 mm, diameter 10 µm, oriented parallelly to the blade trailing edge) and a constant-temperature anemometer system. The calibration of hot-wire probes in the compressible flow of an organic vapor requires substantial efforts, as Hake et al. [17] discussed in more detail. In the present study, a fixed stagnation temperature $T_{o0} = 370$ K during the experiments avoided the need to determine the temperature sensitivity coefficient during calibration. The high wire Reynolds number (of order 1000)

Preprints (www.preprints.org) | NOT PEER-REVIEWED | Posted: 12 September 2023 doi:10.20944/preprints202309.0738.v1

and the fixed wire over-heat ratio of 1.6 ensured that the density and velocity sensitivity coefficients were identical for the used hot-wire probe [17]. That fact made the data reduction and interpretation of the electrical hot wire signals easier, although compressibility effects were present.

3.2. Experimental procedure

Before the experiments, the entire wind tunnel facility was evacuated and then filled with NOVEC 649 mass, yielding the desired density level (so-called inventory forward-control approach). The heating of the wind tunnel using an electrical heating system and the temperature control system working with an additional chiller in the settling chamber enabled a stable total temperature level T_{o0} during the experiments. The temperature drift rate during a measurement campaign was only 10^{-3} K/s. The desired exit Mach number M_2 was mainly controlled by the variable wind tunnel compressor running speed, which was continuously adjustable via the electrical frequency converter. The actual Reynolds number Re was primarily governed by the velocity (i.e., the Reynolds number was strongly linked to the Mach number) and slightly affected by the actual test section density.

Before the experiments with the organic vapor started, tests and instrumentation checks with air at atmospheric conditions were conducted. In the first set of experiments, the pressure measurements, including the traversing of the Pitot probes, were carried out. Based on these data, Mach number, flow velocity, and density were determined utilizing the static pressure, temperature, and mass flow rate data. Then, the Pitot probes were replaced with hot-wire probes, and the hot-wire measurements were carried out at the upstream and downstream stations for the same exit Mach numbers in the second set of experiments. At the central position of the blade passage, the velocity and density data obtained in the first set were used to calibrate the hot-wire probe using a semi-empirical King law (see for details Hake et al. [17]). During the hot-wire measurements, the potential vibration of the probe was checked using a high-speed camera and optical access through a transparent end wall of the cascade. The visual inspection identified a significant probe vibration issue at high subsonic flow ($M_2 > 0.6$) caused by the high dynamic load on the probe stem. The optically determined vibration frequencies acted as outer disturbances while interpreting the hot-wire signals at higher Mach numbers.

3.3. Data Reduction and Uncertainty Analysis

The primary goal of the present study was the determination of the profile loss of the turbine cascade. Among the various methods to express the loss, the present study used the pressure loss coefficient Y

$$Y = \frac{p_{o1} - p_{o2}}{p_{ref}} \tag{1}$$

and the energy loss coefficient ζ

$$\zeta = \frac{h_2 - h_{2s}}{h_0 - h_{2s}} \tag{2}$$

Regarding the reference pressure, p_{ref}, in equation (1), different definitions are available in the literature. Here, the definition $p_{ref} = p_{o2} - p_2$ was used, as proposed by Horlock [18]. The definition of the energy loss coefficient followed Kiock et al. [11]. Averaging of the pressure loss coefficient was performed using the mass-flow averaging procedure for the total pressure difference, as Horlock [18] described. The average reference pressure was obtained by the mass-flow averaged total exit pressure value and the area-averaged static exit pressure value. A similar procedure was applied for the averaged energy loss coefficient ζ.

The energy loss coefficient ζ and the pressure loss coefficient Y were compared and converted using the simple ideal gas relation

$$Y = \zeta \left(1 + \frac{2\gamma - 1}{4} \mathrm{M}_2^2\right) \tag{3}$$

Preprints (www.preprints.org) | NOT PEER-REVIEWED | Posted: 12 September 2023 doi:10.20944/preprints202309.0738.v1

with γ as the isentropic exponent and M_2 as the exit Mach number. It might be noticed that Eq. (3) is the first part of a power series for the Mach number of the exact conversion formula. Its deviation from the precise relationship between ζ and Y involving thermodynamic calculations for the real gas behavior was less than 2% for the present study at the highest Mach number.

All thermodynamic variables were obtained through the fluid database program REFPROP by NIST using the pressure and temperature measurements. For the Pitot probe data reduction, the scheme and the program detailed explained by Schollmeier and aus der Wiesche [19] were applied. The relative uncertainty level of the pressure measurements was of order $\Delta p/p$ = 0.5 % up to 1.6 %. This level was mainly given by bias errors caused by the unknown hydrostatic pressure due to potential condensation in the pressure lines (see reference [16] for a detailed discussion about the issues caused by condensation in pressure lines). The relative temperature uncertainty level was only $\Delta T/T$ = 0.06 % up to 0.1 %. The maximum local pressure coefficient uncertainty was ΔY = 0.0142 (in the wake). A maximum uncertainty of about ΔY_{av} = 0.006 was achieved for the averaged loss coefficients due to the large number of sampling data for averaged quantities. The relative uncertainty levels for Reynolds and Mach numbers were 1 %.

4. Considered literature loss models

Among the many different loss models and correlations available in the open literature, the following frequently used and representative loss models were selected:

- Soderberg's correlation (see Horlock [18] or Dixon and Hall [20])
- Ainley & Mathieson [1]
- Kacker & Okapuu [8]
- Traupel [14]
- Baljé & Binsley [21]

Although the considered loss models are somewhere old-dated, they are still in use in industry and academia. Furthermore, using a modern loss correlation would not provide an advantage for the present airfoil designed by methods of the late 1960s. The selection of the loss models covered the two empirical classical approaches by Soderberg and Ainley & Mathieson (and its follow-up by Kacker & Okapuu) as well as the analytical boundary layer flow approach represented by the loss model proposed by Baljé & Binsley. The Traupel loss model might be considered a practical combination of empirical and analytical data. It is provided in parts in graphical form. For a deeper discussion of potential Reynolds number and roughness effects and for predicting the trailing edge loss contribution, Denton [22], Aungier [6], and Cheon et al. [23] were consulted as sources, too.

Soderberg proposed a relatively simple method for estimating turbine cascade losses in the late 1940s [18,20]. His correlation was intended to predict the total loss for turbine cascades, but considering the limit case for an infinite blade height $b/H \rightarrow 0$ can predict profile losses, including trailing edge losses [18]. The Soderberg correlation is essentially a quadratic function of the deflection angle $\varepsilon = \beta_1 + \beta_2$, and the Reynolds number correction follows the power law with $Re^{-1/4}$. In its original version, no roughness effects were included.

Ainley and Mathieson reported a method of estimating the performance of axial flow turbines in the early 1950s [1,18,20] based on individual loss contributions (profile loss, secondary loss, and tip clearance loss). Their approach has been widely used ever since, and several authors (e.g., [4,6,8]) modified their basic scheme but kept the main ideas. Ainley & Mathieson obtained their loss data for a nominal Reynolds number $Re_2 = 2 \times 10^5$, and they recommended that the total-to-total efficiency η_{tt} of the turbine stage should be corrected for lower Reynolds numbers accordingly to

$$1 - \eta_{tt} \sim Re_2^{-1/5}. \quad (4)$$

Compressibility and roughness effects were not included in the original version of the Ainley and Mathieson correlation. Kacker and Okapuu [8] modified the Ainley and Mathieson loss system, among other things, by reducing the profile loss base level by a factor of three, introducing compressibility effects, and modifying the Reynolds number correction.

Preprints (www.preprints.org) | NOT PEER-REVIEWED | Posted: 12 September 2023 doi:10.20944/preprints202309.0738.v1

A profile loss correlation proposed by Baljé and Binsley [21] was selected to represent a loss model based on the boundary-layer theory. Their profile loss coefficient ζ includes the trailing edge loss. The profile loss can be obtained by the boundary-layer theory expression

$$\zeta = 1 - \frac{\left(\frac{\cos^2\beta_2 \left(1 - \delta * - \theta * - \frac{t_{TE}}{t}\right)^2}{\left(1 - \delta * - \frac{t_{TE}}{t}\right)^2} + \sin^2\beta_2 \left(1 - \delta * - \frac{t_{TE}}{t}\right)^2 \right)}{1 + 2\sin^2\beta_2((1 - \delta * - t_{TE}/t)^2 - (1 - \delta * - \theta * - t_{TE}/t))}. \quad (5)$$

Here, θ^* denotes the normalized boundary layer momentum thickness quantity $\theta^* = (\theta/(t \sin\beta_2)$, and $\delta^* = H\theta^*$ can be computed using the shape factor H of the boundary layer. For turbulent flow, a value of H = 1.4 was used. The Reynolds number correction is implemented via the correlation for the momentum thickness θ. The latter depends on the blade angles and Re. In its original version, roughness effects were not explicitly covered but could be introduced by modifying the boundary layer quantities δ^* and θ^* utilizing suitable roughness correlations [14,24]. The pure boundary layer loss ζ_{BL} can be estimated using a vanishing trailing edge thickness ($t_{TE} = 0$) in Eq. (5).

5. Results and Discussion

The actual turbine cascade consisted of only three full airfoils, see Figure 4. Hence, it was necessary to check the periodicity for the central airfoil where the flow measurements and loss determinations were mainly performed. The exit domain and the guiding side contours were developed based on prior computational fluid dynamics solutions. The static pressure measurements downstream of the central airfoil indicated a high degree of periodicity: $p_2(y)$ was essentially identical to $p_2(y+t)$ at different traverse positions y (the deviations between the pressure measurements were within the experimental uncertainty level). The inflow uniformity was checked using a Pitot probe traversed at the upstream station. It was found that the total pressure $p_{o1}(y)$ remained essentially constant, as reported in the previous study [13].

Figure 5 shows an example of the measured total pressure and turbulence intensity distributions downstream of the central blade obtained for an exit Mach number of $M_2 = 0.68$. Similar results were obtained for other exit Mach numbers M_2 or Reynolds number levels. The wake downstream of the airfoil's trailing edge is expressed by the local total pressure difference distribution $\Delta p_o(y) = p_{o1} - p_{o2}$ (black dots in Figure 5) because the upstream total pressure p_{o1} was constant along the corresponding inflow traverse coordinate y. The grey squares in Figure 5 represent the measured normalized downstream turbulence intensities obtained by the hot-wire anemometry (HWA). Here, the measured data were corrected concerning the finite wire length which is described in more detail in [25]. The agreement between the new HWA turbulence data for NOVEC 649 with the literature data [26] obtained by laser-Doppler anemometry (LDA) for air was reasonable. This agreement supports the hypothesis that real gas effects are not dominating the turbulence at this Mach number level.

The averaged profile loss coefficient ζ is plotted against the exit Reynolds and Mach numbers in Figure 6. In addition to the new experimental data obtained for NOVEC 649, literature data (see Kiock et al. [11]) obtained for air at a fixed Reynolds number $Re_2 = 0.8\times10^6$ but for various Mach numbers M_2 are shown in Figure 6 for a better orientation. The literature loss data in Figure 6 correspond to smooth airfoils, whereas the new NOVEC 649 data were measured for a rough blade ($k_s/c = 4\times10^{-4}$).

Preprints (www.preprints.org) | NOT PEER-REVIEWED | Posted: 12 September 2023 doi:10.20944/preprints202309.0738.v1

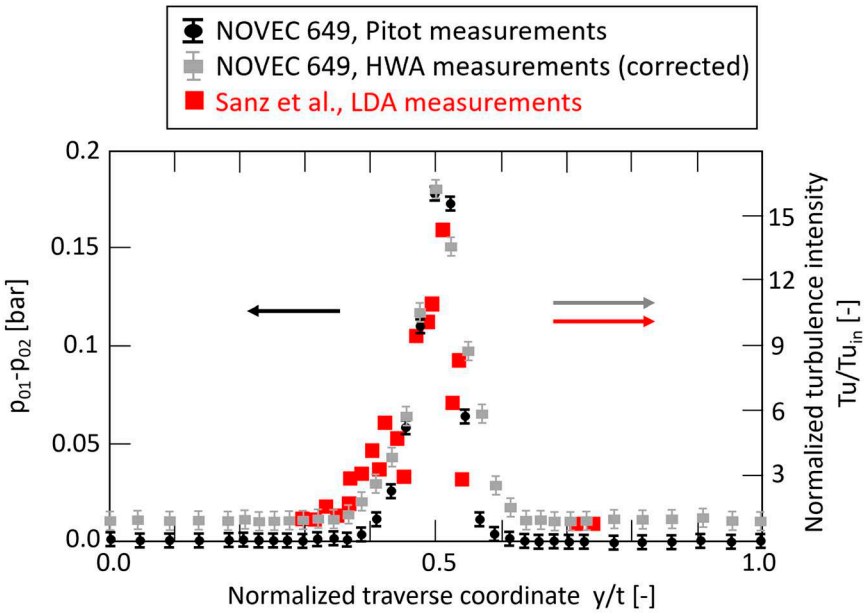

Figure 5. Total pressure and turbulence distributions (NOVEC 649, $M_2 = 0.68$, $Re_2 = 3.2 \times 10^6$).

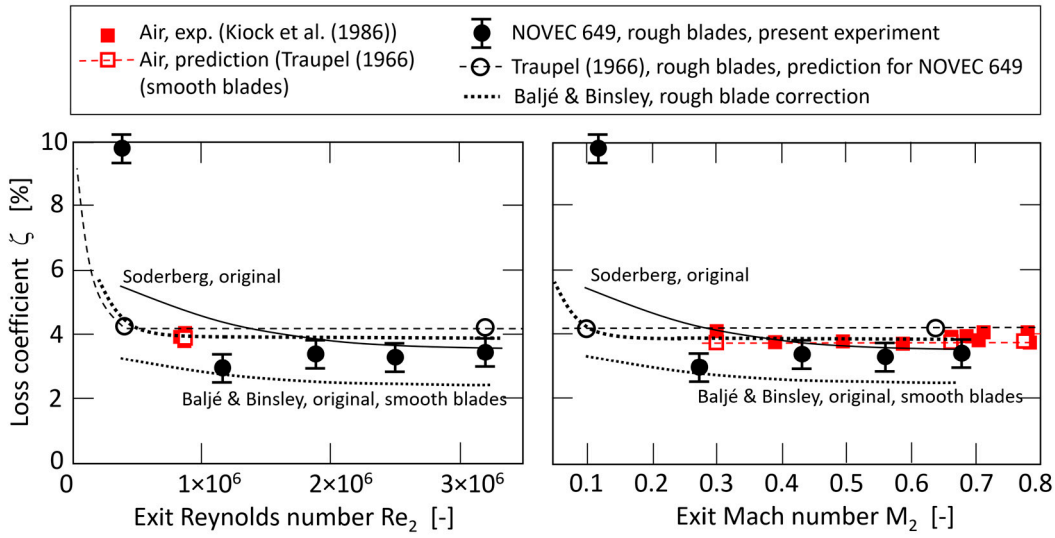

Figure 6. Loss coefficient ζ against exit Reynolds and Mach numbers. The predictions of the correlations for NOVEC 649 are shown in black and correspond to the actual Reynolds and Mach numbers. The literature data for air are shown in red.

The prediction of the Traupel [14] loss system is plotted as empty red symbols in Figure 6, too. In the case of air and smooth blades (red symbols in Figure 6), the agreement between the literature data and Traupel's prediction is excellent. The Reynolds number effect (i.e., an increase of loss for decreasing Reynolds number) was predicted by Traupel for exit Reynolds numbers $Re_2 < 0.5 \times 10^6$. Interestingly, the NOVEC 649 data point obtained for such a Reynolds number exhibited a significant increase of loss in comparison to the relatively stable loss level obtained for higher Reynolds numbers. The Reynolds number correction for the Soderberg correlation predicted a slight loss decrease with increasing Reynolds number. The profile loss level predicted by Soderberg was in remarkable agreement with the experimental data obtained for NOVEC 649 at higher Reynolds numbers. The original Baljé & Binsley method for smooth blades underestimated the profile loss for NOVEC 649 and rough airfoils. Still, a roughness correction of the boundary layer quantities (see section 4) led to

Preprints (www.preprints.org) | NOT PEER-REVIEWED | Posted: 12 September 2023 doi:10.20944/preprints202309.0738.v1

a reasonable agreement in Figure 5 (except for the low Reynolds number data point as in case of Traupel).

In Table 2, the predictions of all considered loss models are listed for the literature data point (air, smooth blades, $Re_2 = 8\times10^5$). Table 2 contains a loss breakdown in the boundary layer and trailing edge loss contributions. Table 3 shows the same for NOVEC 649 obtained at $M_2 = 0.68$ and $Re_2 = 3.2\times10^6$ for the rough airfoils.

Table 2. Loss coefficient ζ and loss breakdown for the literature data point (air, smooth, $Re_2 = 8\times10^5$).

Loss model	ζ (profile total)	ζ_{BL} (boundary layer)	ζ_{TE} (trailing edge)
Soderberg	4.80 %	not resolvable	not resolvable
Ainley & Mathieson*	4.87 %	3.72 %	1.15 %
Kacker & Okapuu	5.71 %	2.86 %	2.85 %
Traupel	3.90 %	2.50 %	1.40 %
Baljé & Binsley**	4.03 %	2.83 %	1.20 %
Experiment [11]	3.9 up to 4.0 % ($\pm$ 0.3 %)	not resolvable	not resolvable

* including Reynolds number correction, ** with shape factor H = 2.0 due to laminar boundary layer.

Table 3. Loss coefficient ζ and loss breakdown for NOVEC 649 ($M_2 = 0.68$, $Re_2 = 3.2\times10^6$).

Loss model	ζ (profile total)	ζ_{BL} (boundary layer)	ζ_{TE} (trailing edge)
Soderberg, original	3.56 %	not resolvable	not resolvable
Soderberg*	4.80 %	not resolvable	not resolvable
Ainley & Mathieson*	4.91 %	3.72 %	1.19 %
Kacker & Okapuu	5.27 %	2.42 %	2.85 %
Kacker & Okapuu*	6.28 %	3.43 %	2.85 %
Traupel (rough blades)	4.10 %	2.94 %	1.16 %
Baljé & Binsley (smooth)	2.44 %	1.60 %	0.84 %
Baljé & Binsley* **	3.93 %	2.79 %	1.14 %
Experiment	3.3 % ($\pm$ 0.5 %)	not resolvable	not resolvable

* with modified Re-ks/c-correction, ** with shape factor H = 1.4 due to turbulent boundary layer.

The original loss models from Soderberg, Ainley & Mathieson [1], Kacker & Okapuu [8], and Baljé & Binsley [21] considered only smooth blades. To cover roughness effects, these models were modified using the correction factor for roughness effects proposed by Cheon [23]. The Traupel [14] loss model contained already roughness effects. For the boundary layer calculation required by the Baljé & Binsley [21] method, the same roughness model was used for calculating the momentum thickness. In the case of smooth blades and airflow at a relatively usual Reynolds number level, the Traupel [14] and the Baljé & Binsley [21] profile loss predictions were very close to the experimental value (see Table 2). Significant deviations occurred in the case of a flow of NOVEC 649 through rough blades (see Table 3 or Figure 6). The agreement between the Soderberg [20] correlation and the experimental data for NOVEC 649 at higher Reynolds or Mach numbers is remarkable, but in the case of lower Reynolds numbers, the Soderberg [20] correlation failed. The Traupel [14] and the Baljé & Binsley [21] correlations predicted profile losses for NOVEC 649, which were in the same order as the observed losses. They were able to describe the observed increase at lower Reynolds numbers qualitatively, but they failed regarding the absolute values. It can be argued that flow separation occurred at the rough airfoils at lower Reynolds numbers (see also the observation reported in [27]), and the boundary layer flow models do not adequately cover that phenomenon.

Preprints (www.preprints.org) | NOT PEER-REVIEWED | Posted: 12 September 2023 doi:10.20944/preprints202309.0738.v1

Tables 2 and 3 demonstrate that the trailing edge contribution to the profile loss was considerable. Substantial deviations regarding the trailing edge loss contribution exist for the literature loss correlations. That underlines the importance of more detailed investigations of trailing edge flows. It would be precious to separate the boundary layer profile loss contribution from the trailing edge flow contribution, but the present experimental setup did not permit such a breakdown. Some base pressure measurements and hot-wire anemometry (HWA) investigations were conducted in the present study. Figure 7 (left) shows a fast Fourier transform (FFT) generated power spectrum density (PSD) sample obtained for NOVEC 649. The recorded hot-wire signals served as basis for the PSD. Since the focus was on the determination of the vortex shedding frequencies, no further correction schemes for the hot-wire signal were necessary to identify the characteristic vortex shedding frequencies f_{TE}. Clearly, the vortex shedding frequency f_{TE} (1x) and its double (2x) can be seen in the spectrum of the hot-wire signal in Figure 7. Since the hot-wire anemometry is not sensitive against the flow direction, the double of the vortex shedding frequency occurred in the spectrum. Based on the fundamental trailing edge vortex shedding frequencies, the corresponding Strouhal number

$$\mathrm{St} = \frac{f_{TE} \cdot t_{TE}}{u} \tag{6}$$

was calculated and plotted against the exit Reynolds number in Figure 7 (right). Literature data [28] obtained for air and the same cascade (with a rounded trailing edge) are plotted in Figure 7, too.

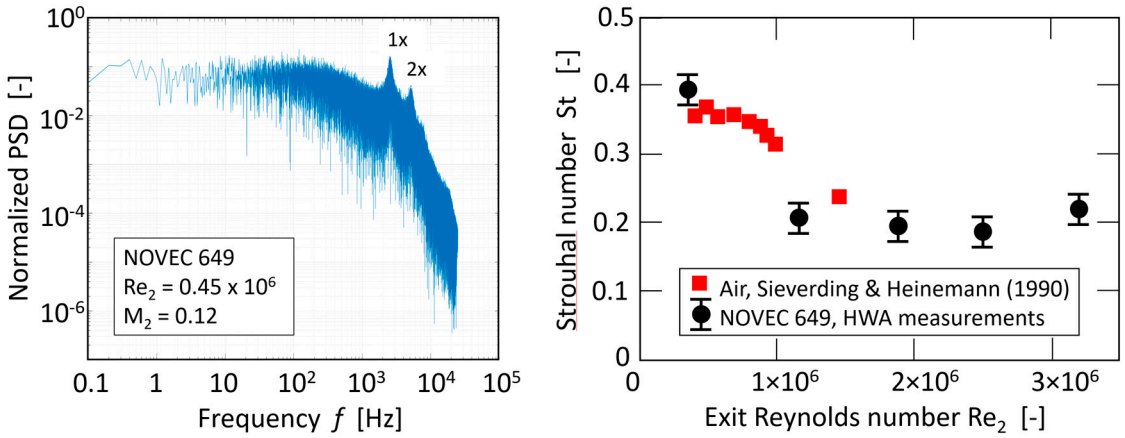

Figure 7. Sample power density spectrum obtained downstream of the trailing edge (left) and vortex shedding Strouhal number against exit Reynolds number (right).

The present experimental data for NOVEC 649 agreed with the literature from Sieverding & Heinemann [28]. It should be remarked that the present NOVEC 649 measurements covered an exit Mach number range of $M_2 = 0.1$ up to 0.7, whereas Sieverding & Heinemann [28] considered $M_2 = 0.3$ up to 0.9. Due to the high density of NOVEC 649, the present Reynolds number range was larger, but still comparable with the literature data. The new data supported the hypothesis that the Reynolds number is the dominant quantity for the vortex shedding frequency and not the Mach number. For higher Reynolds numbers, the Strouhal number was of order 0.2, as observed by Sieverding and Heinemann, whereas a substantially higher Strouhal number was noticed for lower Reynolds numbers. Future research is needed to extract the role of compressibility (i.e., the Mach number) on the trailing edge vortex shedding and its loss contribution.

The measured base pressure coefficient $C_{p,bp} = (p_{TE} - p_2)/(p_{o2} - p_2)$ at the trailing edge was about –0.05 + 0.01 at $M_2 = 0.68$ which was in agreement with the literature data obtained for air (Kiock et al. [11]). This observation indicated that real gas effects are not of primary relevance to trailing edge vortex shedding for the actual subsonic flow. For lower exit Mach numbers, $M_2 < 0.52$, the base pressure coefficient was close to zero (with a tendency to increase slightly for M_2 tending to zero).

An interesting question is whether specific loss models are needed for real gas flows instead of the conventional loss systems obtained for ideal gas flows. At present, the few available data do not

 doi:10.20944/preprints202309.0738.v1

permit a final statement. Future research and an extension of cascade configurations are needed to close that gap. However, the present study represents a first step in this direction and can serve as a case study.

6. Conclusions

Based on the conducted experimental case study using rough blades and the organic vapor NOVEC 649 under subsonic flow conditions, the following conclusions can be drawn:

Whereas specific literature correlations (e.g., Traupel [14]) can predict reasonably profile losses for smooth blades, accounting for roughness effects is still challenging. However, boundary layer theory models (e.g., Baljé & Binsley [21]) have a high potential for predicting profile losses for non-separated flows. In any case, careless use of classical loss models (e.g., Soderberg [18,20], Ainley & Mathieson [1], Kacker & Okapuu [8], Aungier [6]) should be avoided for organic vapor flows in turbomachinery without further experimental proof or validation even for subsonic flow. Based on the present case study, using the simple, robust Soderberg correlation for preliminary design is not worse than considering more sophisticated loss systems like Kacker and Okapuu [8] or Aungier [6].

Significant loss prediction deviations can occur with respect to the trailing edge contribution. For a relatively thick trailing edge, some of the loss models predicted relatively high contributions, which seemed to be questionable (e.g., Kacker & Okapuu [8]). It was found that the exit Reynolds number governed the vortex shedding frequency, and dominant compressibility effects were not observed for $M_2 < 0.68$. This supports the hypothesis that boundary layer flow features characterized by the Reynolds number, not compressibility effects, are the dominating features for trailing edge vortex shedding under subsonic flow conditions. In the case of higher Mach numbers, transonic vortex shedding and compressibility effects and acoustics waves might substantially contribute to the profile loss.

Author Contributions: For research articles with several authors, a short paragraph specifying their individual contributions must be provided. The following statements should be used "Conceptualization, L.H. and S.a.d.W.; methodology, S.a.d.W.; software, S.S; validation, L.H., S.S. and S.a.d.W.; formal analysis, L.H.; investigation, L.H.; resources, S.a.d.W.; data curation, L.H.; writing—original draft preparation, S.a.d.W.; writing—review and editing, L.H. and S.a.d.W.; visualization, L.H.; supervision, S.a.d.W.; project administration, S.a.d.W.; funding acquisition, S.a.d.W. All authors have read and agreed to the published version of the manuscript.".

Funding: This work is part of the German-Franco research project "REGAL-ORC" funded by the DFG and the ANR under the DFG grant Wi 1840.

Institutional Review Board Statement: Not applicable.

Data Availability Statement: Data sharing not applicable.

Acknowledgments: The support of Leon Cakievski and Joshua Bäumer during the experiments is highly appreciated.

Conflicts of Interest: The authors declare no conflict of interest.

Nomenclature

b	axial chord	m
c	chord	m
$C_{p,bp}$	base pressure coefficient	-
f	frequency	Hz
H	shape factor	-
H	span	m
h	specific enthalpy	J/kg
k_s	sand grain roughness	µm
M	Mach number	-
$\dot{m}$	mass flow rate	kg/s
o	throat	m

p	pressure	Pa
u	flow velocity	m/s
Re	Reynolds number	-
s	specific entropy	J/(kg·K)
St	Strouhal Number	-
T	temperature	K
t	spacing	m
t_{TE}	trailing edge thickness	m
x	axial coordinate	m
y	vertical traversing coordinate	m
Y	pressure loss coefficient	-
Z	compressibility factor	-

Greek Symbols

β	flow angle	°
δ	boundary layer thickness	m
Γ	fundamental derivative of gas dynamics	-
Λ	turbulent length scale	m
ζ	energetic loss coefficient	-
ε	deflection	°
θ	momentum thickness	m
η	dynamic viscosity	Pa·s
η_{tt}	total-to-total stage efficiency	-
κ	isentropic exponent	-
ρ	density	kg/m³

Subscripts

0	settling chamber
1	inflow (upstream station)
2	exit (downstream station)
av	average
o	total
ref	reference
s	isentropic

References

1. Ainley, D. G., Mathieson, G. C. R., (1951). An Examination of the Flow and Pressure Losses in Blade Rows of Axial-Flow Turbines. NGTE Report R.86, Ministry of Supply, London
2. Harloff, G. J., (1987). Real Gas Properties and Space Shuttle Main Engine Fuel Turbine Performance Prediction. Proceedings ASME Gas Turbine Conference and Exhibition, Anaheim, CA, USA, May 31-June 4, 1987, paper-ID 87-GT-106
3. Macchi, E., Perdichizzi, A., (1981). Efficiency Prediction for Axial-Flow Turbines Operating with Nonconventional Fluids. ASME J. Eng. Power, vol. 103, pp. 718-724
4. Craig, H. R. M., Cox, H. J. A., (1971). Performance Estimation of Axial Flow Turbines. Proc. Instn. Mech. Engrs., vol. 185(32/71), pp. 407-424
5. Da Lio, L., Manente, G., Lazzaretto, A., (2014). New efficiency charts for the optimum design of axial flow turbines for organic Rankine cycles. Energy, vol. 77, pp. 447-459
6. Aungier, R. H., (2006). Turbine Aerodynamics – Axial-Flow and Radial-Inflow Turbine Design and Analysis. ASME Press, New York
7. Sim, J.-B., Yook, S.-J., Kim, Y. W., (2022). Performance Analysis of Organic Rankine Cycle with the Turbine Embedded in a Generator (TEG). Energies, vol. 15, paper 309, 18 pages

8. Kacker, S. C., Okapuu, U., (1982). A Mean Line Prediction Method for Axial Flow Turbine Efficiency. ASME J. Eng. Power, vol. 104, pp. 111-119
9. Chyu, M. K., Young, G. M., (1988). A Performance/Loss Evaluation of SSME HPFTP Turbine. NASA, Report N89-21735, Marshall Space Flight Center
10. Salah, S. I., White, M. T., Sayma, A. I., (2022). A comparison of axial turbine loss models for air, sCO2 and ORC turbines across a range of scales. Int. J. Thermofluids, vol. 15, paper-ID 100156
11. Kiock, R., Lehthaus, F., Baines, N. C., Sieverding, C. H., (1986). The Transonic Flow Through a Plane Turbine Cascade as Measured in Four European Wind Tunnels. ASME J. Eng. Gas Turbines Power, vol. 108, pp. 277-284
12. Baumgärtner, D., Otter, J. J., Wheeler, A. P. S., (2019). The Effect of Isentropic Exponent on Transonic Turbine Performance. Proceedings of the ASME Turbo Expo, Phoenix, AZ, USA, 17–21 June 2019, paper-ID GT2019-90251
13. Hake, L., Reinker, F., Wagner, R., aus der Wiesche, S., Schatz, M., (2022). The Profile Loss of Additive Manufactured Blades for Organic Rankine Cycle Turbines. Int. J. Turbomach. Propuls. Power 2022, 7(1), 11, https://doi.org/10.3390/ijtpp7010011
14. Traupel, W., (1966). Thermische Turbomaschinen. Band 1. Springer-Verlag, Berlin
15. aus der Wiesche, S., Reinker, F., (2022). Dimensional analysis and performance laws for organic vapor flow turbomachinery. Energy, vol. 257, paper 124635
16. aus der Wiesche, S., (2023). Experimental Investigation Techniques for Non-Ideal Compressible Fluid Dynamics. Int. J. Turbomach. Propuls. Power 2023, 8(2), 11; https://doi.org/10.3390/ijtpp8020011
17. Hake, L., Sundermeier, S., Cakievski, L., Bäumer, J., aus der Wiesche, S., Matar, C., Cinnella, P., Gloerfelt, X., (2022). Hot-Wire Anemometry in High Subsonic Organic Vapor Flows. Proc. ASME Turbo Expo 2022, Rotterdam, The Netherlands, paper GT2022-81689
18. Horlock, J. H., (1985). Axial Flow Turbines. Krieger Publishing, Malabar, Florida
19. Schollmeier, J.-N., aus der Wiesche, S., (2022). A user-friendly pitot probe data reduction routine for non-ideal gas flow applications. Energy, vol. 261, Part A, paper 125143
20. Dixon, S. L., Hall, C. A., (2010). Fluid Mechanics and Thermodynamics of Turbomachinery. 6th Edition. Butterworth-Heinemann, Burlington, MA
21. Baljé, O. E., Bisnley, R. L., (1968). Axial Turbine Performance Evaluation. Part A – Loss-Geometry Relationships. ASME J. Eng. Power, October 1968, pp. 341-348
22. Denton, J. D., (1993). Loss Mechanisms in Turbomachines. ASME J. Turbomachinery, vol. 115, pp. 621-656
23. Cheon, J. H., Milcák, P., Pacák, A., Kang, C. R., St'astný, M., (2016). Profile Loss Prediction for High Pressure Steam Turbines. Proc. ASME Turbo Expo 2016, Seoul, South Korea, paper GT2016-56114
24. Gersten, K., Herwig, H., (1992). Strömungsmechanik. Vieweg, Wiesbaden
25. Hake, L., Sundermeier, S., aus der Wiesche, S., Bienner, A., Gloerfelt, X., Matar, C., Cinnella, P., (2022). CFD-supported data reduction of hot-wire anemometry signals for compressible organic vapor flows. Proc. XXVI Biennial Symposium on Measuring Techniques in Turbomachinery, September 2022, Pisa, Italy
26. Sanz, W., Gehrer, A., Woisetschläger, J., Forstner, M., Artner, W., Jericha, H., (1998). Numerical and experimental investigation of the wake flow downstream of a linear turbine cascade, Proc. ASME Turbo Expo, 2 – 5 June 1998, Stockholm, Sweden, paper 98-GT-246
27. Yuan, L. Q., Kind, R. J., (2006). Measurements and computations of compressible flow through a turbine cascade with surface roughness, Proc. ASME Turbo Expo, 8 – 11 May 2006, Barcelona, Spain, paper GT2006-90018
28. Sieverding, C. H., Heinemann, H., (1990). The Influence of Boundary Layer State on Vortex Shedding from Flat Plates and Turbine Cascades. ASME J. Turbomachinery, vol. 112, pp. 181-187